

等离子束表面冶金 $(Cr, Fe)_7C_3/\gamma-Fe$ 金属
陶瓷复合涂层工艺

刘均波

(潍坊学院 机电系, 山东 潍坊 261061)



刘均波

摘 要: 研究了工艺参数对等离子束表面冶金涂层的影响。当工作电流降低或扫描速度增加时, 冶金层组织趋于细化。由此确定最佳工作电流值为 300 A, 扫描速度为 500 mm/min。采用优化的工艺参数, 以 Fe—Cr—C—Nb—Al 粉末为原料, 在 Q 235 钢表面制得以原位生成 $(Cr, Fe)_7C_3$ 为增强相, 以 $\gamma-Fe$ 固溶体与少量 $(Cr, Fe)_7C_3$ 构成的共晶为基体的复合涂层。涂层组织致密, 与基材完全冶金结合。

关键词: 等离子束表面冶金; 工艺参数; 显微组织; 显微硬度

中图分类号: TG174.44 文献标识码: A 文章编号: 0253-360X(2007)04-017-04

0 序 言

等离子束表面冶金技术是一项新兴的零件加工与表面改性技术, 能极大地提高零件表面的硬度、耐磨、耐腐蚀、耐疲劳等性能, 具有工件扭曲变形较小、过程易于实现自动化控制、生产效率高等优点而在工业上展现出广阔的应用前景。现已成功应用在矿山机械易损件如煤矿井下刮板运输机中部槽和采煤机截齿中。另外, 还可利用该技术对失效的零件进行修复, 大量节约加工成本^[1-4]。

$(Cr, Fe)_7C_3$ 金属陶瓷具有硬度高、耐腐蚀性及抗氧化性等优点, 常被用作耐磨涂层的增强相^[5,6]。固溶了大量合金元素的 $\gamma-Fe$ 固溶体具有良好的塑性、韧性及较高的强度, 以 $(Cr, Fe)_7C_3$ 金属陶瓷作为增强相, 以 $\gamma-Fe$ 固溶体作为基体的 $(Cr, Fe)_7C_3/\gamma-Fe$ 复合材料涂层, 可望具有优异耐磨损性能。

作者重点讨论了等离子束表面冶金工艺参数对冶金层组织性能的制约关系, 获得了等离子束表面冶金 $(Cr, Fe)_7C_3/\gamma-Fe$ 金属陶瓷复合材料涂层的最佳工艺参数。

1 试验材料与方法

等离子束表面冶金基材为 Q235 钢, 试样尺寸为 50 mm×20 mm×10 mm。试验采用廉价的 Fe—Cr—

C—Nb—Al 粉末为原料, 其粒度在 -200 ~ +300 目左右。表面冶金用粉末材料为自行设计的铁基自熔性合金粉末, 其化学成分为: Fe 58.5%—Cr 35%—C 4.5%—Nb 1%—Al 1%。

试验设备采用 DRF—1 型全自动负压等离子束表面冶金数控设备, 原理如图 1 所示。等离子束表面冶金工艺参数为: 工作电压 30 V, 送粉量 30 g/min, 扫描速度 300 ~ 800 mm/min, 工作气体 (Ar) 流量 2.5 L/min, 送粉气体 (Ar) 流量 3 L/min。沿等离子束扫描的垂直方向切取截面并制得金相试样, 试样经王水深腐蚀后, 用 Nephot II 型光学金相显微镜和 JSM—5800 型扫描电子显微镜观察显微组织; 采用日本理学 Dmax—2200pc 旋转阳极 X 射线衍射仪并结合 S—530 型 LinkISIS 能谱仪进行物相鉴定; 冶金层及基材的显微硬度用 HVS1000 型显微

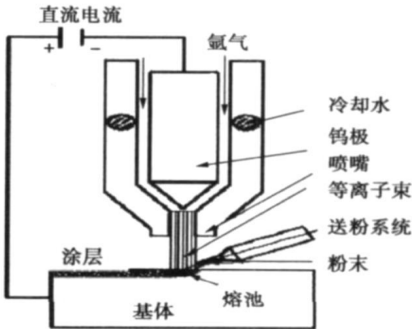


图 1 等离子束表面冶金原理图

Fig. 1 Schematic drawing of plasma surface metallurgy

硬度计测量, 载荷为 100 g。

2 结果与讨论

工艺参数优化一直是等离子束表面冶金技术中的主要研究课题。良好的等离子束表面冶金层应该是表面光滑、无裂纹, 且基体与冶金层界面为冶金结合。研究表明, 影响等离子束表面冶金因素很多, 如材料特性、环境条件等。但在等离子束表面冶金过程中实际可调的参数并不多, 这是因为, 基体材料及粉末材料是根据工况并考虑工艺特点而选定的, 等离子束表面冶金的质量主要靠调整等离子束功率、工作电流与电压、扫描速度等几个参数来实现。这些参数都将影响粉末的加热状态, 进而影响冶金层的宏观及微观质量。

2.1 工作电流的影响

在工作电压一定的情况下, 等离子束功率由工作电流表征, 工作电流大则等离子束功率大, 工作电流小则等离子束功率小。

工作电流的变化对显微组织结构有着明显的影响。图 2 为不同工作电流下冶金层的显微组织。在外界环境不变的情况下, 工作电流较大 (450 A), 输给冶金层的热量增大, 导致熔池中温度较高, 熔池的冷却速度就会很低, 凝固后晶粒粗大。另外, 基体熔化量增多, 熔化了基体材料通过熔池中的对流传质作用, 扩散到涂层中, 还会使涂层中的组成元素蒸发和分解, 造成过烧现象, 从而使冶金层成分远离涂层设计成分, 达不到性能要求。在工作电流为 300 A 时, 生成的组织比较细小, 晶间距离也较小。而当电流较小 (如 $I < 250$ A) 时, 表面涂层熔化而基体不熔化, 涂层在金属表面呈“液珠”状态, 润湿性差, 表面“液珠”不能在金属表面铺展, 凝固后在金属表面形成“铁豆”。

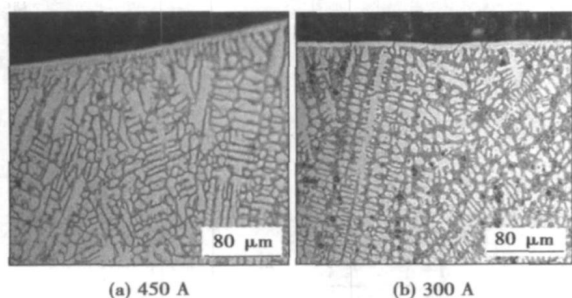


图 2 不同工作电流下冶金层组织

Fig. 2 Microstructure of coatings with different working current

2.2 扫描速度的影响

在等离子束表面冶金过程中, 等离子束扫描速度对冶金层的质量也有很大的影响。当等离子束输出功率和光斑直径一定时, 扫描速度的大小在很大程度上代表等离子束能量效应。等离子束与材料的交互作用时间由扫描速度决定。

图 3 为不同扫描速度下冶金层的显微组织。由图可以看出, 扫描速度越大, 交互作用时间越短, 注入材料的能量也就越少, 当其增大到一定值时, 熔化的深度低于涂层的厚度, 此时, 等离子束输出功率不足以使粉末材料全部熔化, 即使粉末发生了完全的熔化, 但由于熔体表面张力较大, 冷却时呈聚集收缩状态, 也不能形成连续均匀的涂层, 涂层与基体之间不能实现冶金结合, 结合强度也就相当低, 不能满足实际的应用要求。随着扫描速度的增加, 冶金层组织趋于细化, 其原因是随扫描速度的增加, 等离子束在试样表面上停留的时间越短, 基体吸收的能量就越少, 在同样的传热条件下, 冷却速度就越快, 熔池中的晶粒来不及长大就被凝固。但扫描速度过大, 基体吸收的能量就少, 导致合金粉末中有些颗粒来不及熔化, 见图 3c。

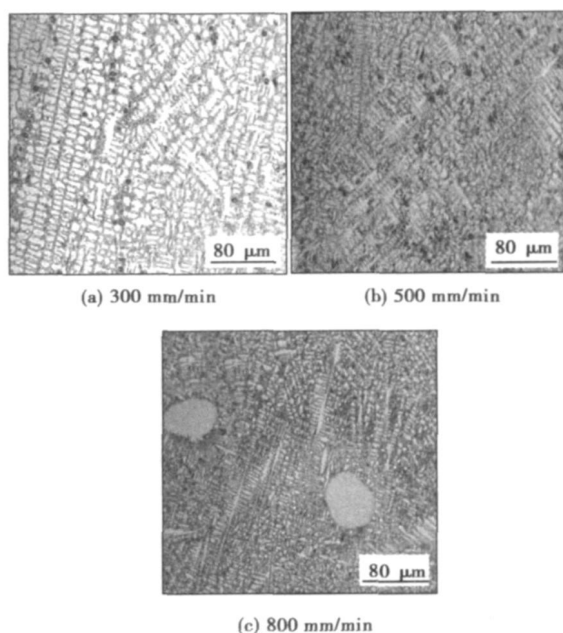


图 3 不同扫描速度下冶金层的组织

Fig. 3 Microstructure of coatings with different scanning speed

2.3 等离子束表面冶金 $(\text{Cr, Fe})_7\text{C}_3/\gamma\text{-Fe}$ 金属陶瓷复合材料涂层的典型组织和硬度分布

通过上述分析, 确定等离子束表面冶金最佳工艺: 工作电流为 300 A, 扫描速度为 500 mm/min。由此获得等离子束表面冶金 $(\text{Cr, Fe})_7\text{C}_3/\gamma\text{-Fe}$ 金属陶瓷

复合材料涂层, 其 X 射线衍射结果(图 4)表明, 涂层的主要组成相为 (Cr, Fe)₇C₃ 及 γ-Fe 固溶体。

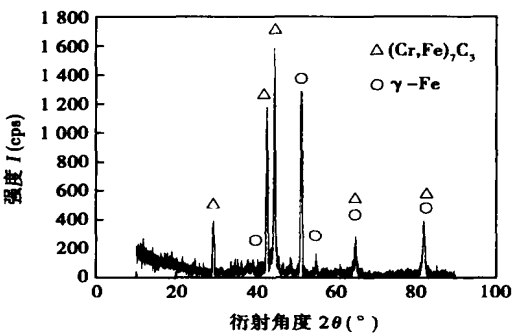


图 4 等离子束表面冶金涂层 X 射线衍射结果
Fig. 4 XRD pattern of coating formed by plasma surface metallurgy

图 5 为涂层显微组织的 SEM 低倍和高倍照片, 可明显看出, 涂层组织均匀细小, 无显微孔洞及裂纹, 涂层显微组织结构为黑色块状初生相均匀分布于均匀细小的灰白色共晶基体上。由 X 射线衍射分析并结合能谱分析结果表明, 黑色规则块状初生相为 (Cr, Fe)₇C₃, 其体积分数约占整个涂层的 50%, 共晶基体中体积分数较高的灰白色长条状组织为 γ-Fe 固溶体, EDS 分析结果表明 γ-Fe 固溶体中固溶有大量 Cr, 共晶基体中长条组织之间的黑色不规则粒状组织为共晶 (Cr, Fe)₇C₃。可见, 等离子束表面冶金 (Cr, Fe)₇C₃/γ-Fe 金属陶瓷复合涂层为以原位生成初生相 (Cr, Fe)₇C₃ 为增强相、以 γ-Fe 固溶体与少量 (Cr, Fe)₇C₃ 构成的共晶为基体的复合材料涂层。

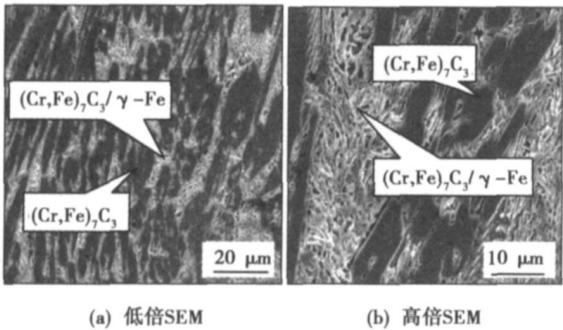


图 5 等离子束表面冶金 (Cr, Fe)₇C₃/γ-Fe 金属陶瓷复合材料涂层显微组织
Fig. 5 SEM microstructure of (Cr, Fe)₇C₃/γ-Fe ceramal composite coating formed by plasma surface metallurgy

图 6 为等离子束表面冶金 (Cr, Fe)₇C₃/γ-Fe 复合材料涂层与基材结合区显微组织扫描电镜照片。

可以看出, 涂层与基材结合区部位有一条明显的白亮带, 能谱分析结果表明, 白亮带的主要成分为 Cr 和 Fe, 可见涂层与基材结合区部位在成分上进行了充分的混合, 结合区的局部位置, 组织有明显的由基体到涂层外延生长的特征, 这说明, 结合区部位的基材在冶金过程中固溶了大量的 Cr, 在随后的冶金熔池极快速冷却过程中以 γ-Fe 固溶体形式保持到室温, 并且基材上的 γ-Fe 固溶体树枝晶由基材外延生长至涂层内部。可见, 涂层与基材之间形成了良好的冶金结合。

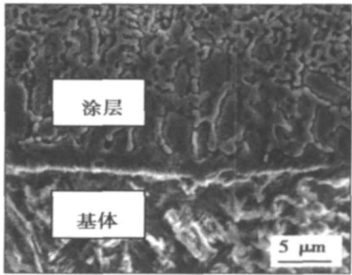


图 6 等离子束表面冶金 (Cr, Fe)₇C₃/γ-Fe 金属陶瓷复合材料涂层与基材结合区的显微组织
Fig. 6 SEM microstructure of bonding zone of (Cr, Fe)₇C₃/γ-Fe ceramal composite coating formed by plasma surface metallurgy

图 7 为等离子束表面冶金 (Cr, Fe)₇C₃/γ-Fe 复合材料涂层的显微硬度分布曲线。可见, 由表层到基体, 涂层显微硬度梯度分布合理。表层硬度较高, 平均约 930 HV, 这是由于表层初生增强相 (Cr, Fe)₇C₃ 的含量较高, 而 (Cr, Fe)₇C₃ 是密排六方点阵结构, 具有较高的显微硬度(约 1300 HV 左右); 靠近结合区的部位涂层硬度较低, 这是由于该部位初生增强相 (Cr, Fe)₇C₃ 的含量较低的缘故。

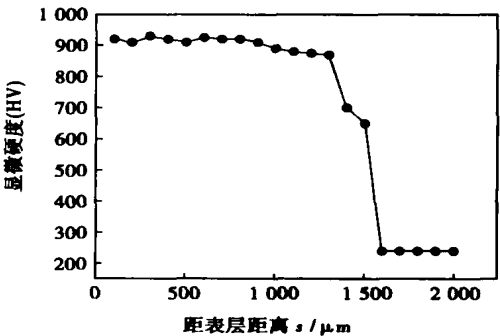


图 7 等离子束表面冶金 (Cr, Fe)₇C₃/γ-Fe 金属陶瓷复合材料涂层的显微硬度
Fig. 7 Microhardness of (Cr, Fe)₇C₃/γ-Fe ceramal composite coating formed by plasma surface metallurgy

3 结 论

- (1) 当工作电流增加或扫描速度降低时, 等离子束表面冶金层的冷却速度降低, 凝固后晶粒粗大; 当工作电流降低或扫描速度增加时, 等离子束表面冶金层冷却速度增加, 组织趋于细化。由此确定等离子束表面冶金最佳工作电流为 300 A, 扫描速度为 500 mm/min。
- (2) 以廉价的 Fe—Cr—C—Nb—Al 粉末为原料, 采用等离子束表面冶金技术, 在 Q235 钢表面制得以原位生成 $(Cr, Fe)_7C_3$ 为增强相, 以 γ -Fe 固溶体与少量 $(Cr, Fe)_7C_3$ 构成的共晶为基体的复合材料涂层。
- (3) 该涂层组织细密, 无显微孔洞及裂纹, 与基材之间形成了良好的冶金结合。

参考文献:

[1] 李惠琪, 李惠东, 李 敏, 等. DC—Plasma—Jet 表面冶金技术研究[J]. 材料导报, 2004 18(10): 194—197.

[2] 李 敏, 李惠东, 李惠琪, 等. 等离子体表面改性技术的发展[J]. 金属热处理, 2004 29(7): 5—9.

[3] Li Huiqi, LIU Bangwu, LI Huidong, *et al.* Study on cracking behavior of plasma surface metallurgy Fe—based layer[A]. 14th IFHTSE Congress, 2004.

[4] 刘邦武, 李惠琪, 张丽民, 等. 等离子束表面冶金过程研究[J]. 材料导报, 2004 18(10): 192—195.

[5] Liu J B, Huang J H, Wang L M. Study on PTA clad $(Cr, Fe)_7C_3/\gamma$ -Fe ceramal composite coating[J]. Acta Metallurgica Sinica (English letters), 2005 18(6): 695—700.

[6] 刘均波, 王立梅, 黄继华. 等离子束表面冶金 Cr_7C_3/γ -Fe 金属陶瓷复合材料涂层组织与耐蚀性[J]. 金属热处理, 2006, 31 (3): 34—36.

作者简介: 刘均波 男, 1973 年出生, 博士, 副教授。主要从事表面涂层技术和粉末冶金方面的研究工作, 发表论文 10 余篇。

Email: junboliu0525@163.com

finite element numerical simulation

Process of $(\text{Cr}, \text{Fe})_7\text{C}_3/\gamma\text{-Fe}$ ceramal composite coating formed by plasma surface metallurgy LIU Junbo (School of Mechanical and Electronic Engineering, Weifang University, Weifang 261061, Shandong, China). p17—20

Abstract The effect of process parameters on the $(\text{Cr}, \text{Fe})_7\text{C}_3/\gamma\text{-Fe}$ ceramal composite coating formed by plasma surface metallurgy on Q235 steel substrate was researched. With the increase of scanning speed or decrease of working current, microstructure of coating was refined. Therefore, it can be ascertained that the optimum working current is 300 A and the optimum scanning speed is 500 mm/min. A in situ reinforcing phase $(\text{Cr}, \text{Fe})_7\text{C}_3$ ceramal composite coating was fabricated on substrate of Q235 steel by plasma surface metallurgy with the Fe-Cr-C-Nb-Al alloy powders. The ceramal composite coating has a rapidly solidified microstructure consisted of primary $(\text{Cr}, \text{Fe})_7\text{C}_3$ and the $(\text{Cr}, \text{Fe})_7\text{C}_3/\gamma\text{-Fe}$ eutectics, and is metallurgically bonded to Q235 steel substrate.

Key words: plasma surface metallurgy; process parameters; microstructure; microhardness

Modelling and simulation of resistance spot welding inverter

JI Chuntao, PENG Xin, LUO Xianxing, DENG Lipeng (Material Science and Engineering School, Nanchang Institute of Aeronautical Technology, Nanchang 330034, China). p21—24

Abstract: The simulation tool in Matlab was used to characterize the resistance welding inverter system and to optimize the circuit parameters. The system output waveforms were analyzed and simulated for different filter capacitors and secondary loads. The result shows that the filter capacitor should be selected so that the rectifier output current is intermittent pulsative, and load current is supplied by the rectifier at voltage crest and by the capacitor at voltage trough. The secondary current rises as exponential function and its rising rate is a inverse proportional to the secondary inductance. It will finally reach a maximum value which is not affected by the inductance when provided the welding time is long enough.

Key words: resistance welding; inverter; system simulation

Microstructure and properties of welded joint for narrow gap laser welding of 42CrMo steel bevel gear shaft WU Shikai, YANG Wuxiong, DONG Peng, XIAO Rongshi (National Center of Laser Technology, Beijing University of Technology, Beijing 100022, China). p25—28

Abstract: The manufacturing of a heavy type bevel gear shaft is generally machined separately, and then jointed by welding. Aimed to the joining of the quenched and tempered 42CrMo steel bevel gear shafts for a heavy-duty machine, a 3500 W Slab CO_2 laser was applied and narrow gap laser welding process was adopted with filler wire of TGS—2CM. Meanwhile, the performance and

metallographic structure of the joint were studied. The experiment results demonstrate that there are no cracks and porosities in the joint even without preheating and postweld heat treatment when the appropriate laser welding parameters are used. The microstructure in the weld and heat-affected zone is fine bainite. The micro-hardness of fusion area is about 580HV0.2, and no apparent softened zone exists in the welded joint. The tensile strength of the joint is in 980—1080 MPa and equivalent to that of the base material, which is satisfied with the service demand.

Key words: laser welding; narrow gap; 42CrMo steel; bevel gear shaft; joint properties

A—TIG welding of magnesium alloy with activating welding wire LIU Liming, CAI Donghong, ZHANG Zhaodong, ZHU Meili (State Key Laboratory of Materials Modification & School of Materials Science and Engineering, Dalian University of Technology, Dalian 116024, China). p29—32, 37

Abstract Several single common compounds were taken as basic activating fluxes in the tungsten inert gas (TIG) welding process with filler wire. The results indicated that in A—TIG welding of magnesium alloy, the activating fluxes coated on the welding wire can also increase weld penetration. The chloride shows a prominent effect on the weld penetration, and the penetration even can be increased 3 times, which compared with the conventional TIG welding with filler wire. The boiling points of the fluxes that increased weld penetration are mostly in the regions about 900 °C. The interdiffusion ability between the droplet metal and the weld pool metal became worse in the TIG welding process with filling activating welding wire than that with the normal wire, and filling ability of the welding wire deteriorates a little, comparing with the normal welding wire.

Key words: activating welding wire; activating fluxes; welding wire filling ability

Microstructure and wear-resisting property of TiC particle reinforced coatings clad by TIG welding with multiple layer

SONG Sili, ZOU Zengda, WANG Xinhong, LI Qingning (School of Materials Science and Engineering, Shandong University, Jinan 250061, China). p33—37

Abstract By using TIG welding, ferrite based composite coating reinforced with TiC has been synthesized by preplaced alloy powder which contains Ti and C on the surface of conventional carbon steel. Results show that in situ TiC particles were prepared in the coating. The microstructure of the coating was mainly composed of ferrite, retained austenite, TiC particles and carbide. The surface hardness of the coating is higher than 55 HRC and presents gradient distribution nearer to the surface of the coating. The wear-resisting test indicated that the friction coefficient of the coating is varied acutely. Blocking effect of TiC particles leads to excellent wearing resistance. The coating has a excellent wear-resisting property. The